Original Paper

Effective dynamic disturbance rejection scheme based on higher order sliding mode control for DC-AC inverter under load variation

Waqas Anjum[1,2] , Abdul Rashid Husain[1], Junaidi Abdul Aziz[1],
Syed Muhammad Fasih ur Rehman[2] , Muhammad Paend Bakht[3] and
Hasan Thaer Alqaraghuli[1]

Abstract
In this paper, a dynamic super twisting sliding mode controller(ST-SMC) is proposed to resolve the problems associated with sudden load changes in AC-DC inverter system such that a high-quality output can be obtained. By developing a non-linear extended state observer (NLESO), both system states and lumped parameter disturbances are estimated and incorporated into controller design. This dynamic disturbance estimation and rejection algorithm not only increases the control loop reliability by eliminating the current sensor dependency, but it also allows the ST-SMC to be implemented with a small switching gain that minimizes the chattering effect. Optimal observer gain parameters design has been achieved by adopting the particle swarm optimization approach. The stability of the entire closed-loop system is proven based on the Lyapunov stability criterion. The effectiveness of the proposed dynamic ST-SMC algorithm has been validated in MATLAB Simulink environment where, the control strategy exhibit rapid dynamic response with a steady-state error of $0V$. The total harmonic distortion (THD) is also reduced to 0.02%% and 0.08%% for linear and non-linear loads, respectively.

Introduction

Voltage source inverter (VSI) is widely employed in power generation systems,[1][3] uninterruptible power supplies,[1,4] electric vehicles systems (EVS),[5] and renewable energy systems,[6,7] in order to supply power to the variety of loads. In these applications, accurate regulation of the inverter output voltage and current are of significant importance. Some of the important factors that degrade the inverter output performance in these applications include inverter non-linear dynamics, sudden load changes, measurements errors, actuator degradation, electromagnetic interference, etc.[1][7] These disturbances cripple the inverter's output voltage and degrade the control performance, which results in high harmonic content and steady-state error in the output[8,9] that may cause damage to the application systems. Therefore, it is important to design an inverter control scheme that will be robust enough to withstand the disturbances resulting from load fluctuations such that the

steady-state error performance can be improved, thereby minimizing the total harmonic distortion.

Up to present, many control approaches have been presented in the literature to handle these disturbances which includes, repetitive control,[10] H_∞ control,[9] model predictive control,[11] backstepping control,[12] fuzzy & neural network-based control,[13,14] and sliding mode control (SMC).[4,6,7] Among these control methods,

[1]School of Electrical Engineering, Universiti Teknologi Malaysia, Johor Bahru, Malaysia
[2]Department of Electronic Engineering, The Islamia University of Bahawalpur, Bahawalpur, Punjab, Pakistan
[3]Balochistan University of Information Technology, Engineering and Management sciences, Quetta, Balochistan, Pakistan

Corresponding author:
Waqas Anjum, Department of Electronic Engineering, Faculty of Engineering, The Islamia University of Bahawalpur, Baghdad Campus, Punjab 63100, Pakistan.
Email: waqas.anjum@iub.edu.pk

SMC is a more favorable control algorithm for the inverter system because of its inherent switching nature[4] that is compatible with VSI gate switching. SMC has superior reference tracking capability and exhibits robustness against disturbances and ensures finite-time convergence. However, it suffers from chattering due to the high switching gain of discontinuous signum function in the control law.[15] Chattering increases the switching losses in the inverter system and injects high-frequency harmonics into the output.[16] In addition, the traditional SMC is normally designed in state feed-back form, which requires comprehensive knowledge of the system parameters and system states.

To mitigate the adverse effects of discontinuous control law, many elegant methods have been presented in the literature. A hysteresis-SMC approach has been presented in Kukrer et al.[17] where a continuous saturation function replaces the discontinuous signum function. However, in this method, there is a trade-off between chattering removal and robustness where large boundary thickness will reduce the chattering but the robustness toward the load variation is decreased.[18] The second approach used for chattering alleviation is gain adaptation. In conventional SMC the switching gain in the controller is required to be larger than the bounds of disturbances in the system to fulfill the existence condition that result in chattering.[15] In adaptive approach the gain over estimation is avoided by appropriately adapting the switching gain proportional to the uncertainties in the system. Adaptive SMC approaches has been presented in Rezkallah et al.[6] and Ghanbarian et al.[19] to improve the steady state performance and THD mitigation in the inverter system. The third approach that is being reported in the literature is to use higher order sliding mode control (HOSMC). The performance of the traditional SMC is restricted by the condition that the system relative degree must be 1 and the inclusion of the switching function in the first derivative of sliding surface. To remove this restriction HOSMC has been proposed in which switching function is included in the higher order derivatives of sliding variables.[20] HOSMC has been implemented on the inverter system in Del Pizzo et al.[21] and Dai et al.[22] to get a continuous control signal by overcoming chattering phenomenon. Although HOSMC approach gives reasonable tracking performance but all of above approaches are designed through state feedback that needs complete information of the system parameters and system states. In addition, the conventional state feedback control laws also lack the ability to deliver superior control performance in the event of the failure of the current sensor to give proper feedback.

Researchers have presented several closed-loop algorithms which do not require any information other than the output of the system. These algorithms are not only straightforward to implement but also utilize fewer sensors. Output feedback SMC schemes have been investigated such as Chang et al.[23] and Zhu et al.[24] but again their gains are designed to be proportional to the uncertainties in the system that causes chattering phenomenon. In Wang et al.[25] output feedback based disturbance and state observer has been proposed to address the harmonic distortion mainly due to the linear load variations. The algorithm can be implemented with relatively low switching gain if the load disturbances are properly estimated however, in order to implement the algorithm comprehensive knowledge of system parameters are required. In Zhao et al.[26] a higher order sliding mode observer based on terminal sliding mode control strategy has been presented. The strategy is model dependent that requires the knowledge of system parameters and additionally the HOSMO performance depends on the bound of the disturbances. In similar scope of study, artificial neural network (ANN) based disturbance rejection SMC is presented in Zhu and Fei[14] where disturbances are estimated using ANN approach are rejected on the sliding surface. It has been noted that disturbances rejection strategies can be implemented by using small controller switching gains and the convergence of states mainly depends upon the convergence of estimation errors. With higher bandwidths of disturbance observers, accuracy of prediction is improved at the expense of amplification of the noise; therefore, the observer gains must be designed appropriately to accomodate these conflicting requirements for optimal system performance. Although output feedback SMC control schemes offers satisfying output, however, the studies in the existing literature concerning dynamic output feedback based continuous higher order SMC for inverter system with mismatched uncertainties are still lacking.

In this paper, a non-linear extended state observer (NLESO) based super twisting control algorithm has been proposed for a single phase inverter with mismatched uncertainties due to a wide range of load variations. The extended state observer estimates the system states along with lumped parameter disturbances. The non-linear terms in ESO contribute toward the convergence of estimation errors while the optimal gain selection has been made using PSO. The estimated states and lumped disturbances are then incorporated in sliding surface and control law. The proposed algorithm can be implemented with small switching gains that effectively reduce the chattering effect without the loss of robustness. The notable merits of this paper are as follows:

- The controller is model-independent, and only the output voltage measurement is required to implement the proposed control law.
- The NLESO proposed here is finite-time convergent and gives robust estimates of system states and accumulates the effects of load disturbances as a lumped parameter. Through the concept of lumped disturbance rejection, the effectiveness of the control law is enhanced and discontinuous control action is eliminated.

- The complexity of observer gain design has been significantly reduced by using PSO technique.

The effectiveness of the proposed algorithm is verified via MATLAB simulations, where the system is subjected to both linear and non-linear load changes.

The rest of the paper is organized as follows: Inverter modeling is given in Section 2. Section 3 deals with the designing of the dynamic ST-SMC control law. Section 4 is devoted to the stability analysis of the proposed algorithm. Observer gain optimization using PSO is described in Section 5 followed by simulation results and discussions in Section 6. Finally, the paper is concluded in Section 7.

Inverter model

A single-phase inverter is shown in Figure 1, where V_{dc} is the *DC* input voltage, *L* is the inductor and *C* is the capacitor that forms the low pass filter whereas S_1, S_2, S_3, S_4 are the semiconductor switches that are controlled by the PWM signal generated based on controller output, *R* describes the variable linear load whereas, u, i_L, i_C, and i_o are the inductor current, capacitor current, and output current, respectively.

Output voltage v_o is taken across the filter capacitor which follows the desired sinusoidal reference voltage. Inverter dynamics by using Kirchhoff's laws are expressed as

$$\begin{cases} \dot{v}_o = \frac{i_L}{C} - \frac{v_o}{RC} \\ \dot{i}_L = \frac{uV_{dc}}{L} - \frac{v_o}{L} \end{cases} \tag{1}$$

For this system, output voltage v_o and inductor current i_L are considered as state variables. In reference tracking, the output voltage v_o is designed in such a way that it is able to track the desired sinusoidal reference even in the presence of linear and non-linear load variations. From (1) it is clear that the load is coupled to the output voltage v_o and inductor current i_L where any variation in the load will affect both of the state variables. By considering the direct coupling between v_o and load variation, the system (1) can be re-expressed as follows:

$$\begin{cases} \dot{v}_o = \frac{i_L}{C} - \frac{v_o}{RC} + d(t) \\ \dot{i}_L = \frac{uV_{dc}}{L} - \frac{v_o}{L} \end{cases} \tag{2}$$

where $d(t) = (\frac{1}{RC} - \frac{1}{R_0 C})v_o$ is the mismatched disturbance that acts on the inverter through the channel that is different from the input channel. R_0 is the nominal value of resistance, v_o is assumed to be the only measurable output that is $y = v_o$ and the control objective is to track a sinusoidal reference voltage v_{ref} such that $v_{ref} - v_o = 0$.
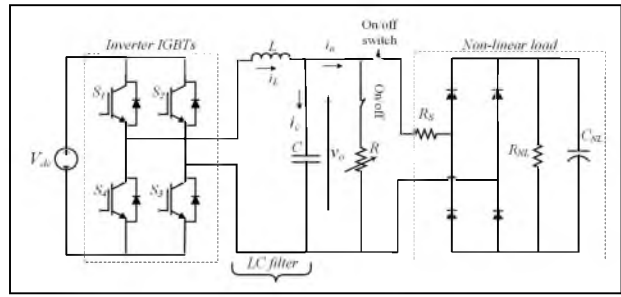

Figure 1. Single phase DC-AC inverter.

Controller design

The main control objective is to develop a robust controller for this VSI system that can track the desired reference sinusoidal voltage v_{ref} with minimized steady-state error and THD in the presence of load variations. In order to transform (2) into a class of non-linear system, the first state is defined as

$$x_1 = v_{ref} - v_0 \tag{3}$$

By taking derivative of (3) and inserting (2), it becomes

$$\dot{x}_1 = \dot{v}_{ref} - \frac{i_L}{C} + \frac{v_o}{RC} + d_1(t) = x_2 \tag{4}$$

where, $d_1(t) = -(\frac{1}{RC} - \frac{1}{R_0 C})v_o$ is the mismatched uncertainty due to load parameter variations. By taking the derivative of (4) it gives

$$\dot{x}_2 = f(t) + bu \tag{5}$$

where $b = -\frac{V_{dc}}{LC}$ and $f(t) = \ddot{v}_{ref} + \frac{v_o}{C}\left(\frac{1}{L} - \frac{1}{R_0^2 C}\right) + \frac{i_L}{R_0 C^2} - \dot{v}_o\left(\frac{1}{RC} - \frac{1}{R_0 C}\right)$ Thus, the inverter system subjected to load uncertainties can be presented, as a class of non-linear dynamic systems which contains the system states as chain of integrals and system uncertainties as lumped parameter, as follows,

$$\begin{cases} \dot{x}_1 = x_2 \\ \dot{x}_2 = f(t) + bu \\ y = x_1 \end{cases} \tag{6}$$

where, x_1, x_2 are state vectors, $f(t)$ is the lumped parameter disturbance that includes both matched and mismatched disturbances, u is the system input while b is the input coefficient. In order to estimate the system states and lumped parameter uncertainty the non-linear extended state observer can be defined as

$$\begin{cases} \dot{z}_1 = z_2 - \beta_1 e_1 \\ \dot{z}_2 = z_3 - \beta_2 fal(e_1, \alpha_2, \delta) + bu \\ \dot{z}_3 = -\beta_3 fal(e_1, \alpha_1, \delta) \end{cases} \tag{7}$$

where $\beta_1, \beta_2, \beta_3$ are the observer gains that need to be designed. $e_1 = z_1 - x_1$ represents estimation error, whereas $fal(*)$ is a continuous function given as

$$fal(e, \alpha, \delta) = \left\{ \begin{array}{ll} \frac{e}{\delta^{1-\alpha_i}} & if \quad |e| \leqslant \delta \\ |e|^{\alpha_i} sign(e) & if \quad |e| > \delta \end{array} \right\}$$

where $i = 1, 2$, $\delta > 0$ is the length of the linear segment in the neighborhood of origin and $1 > \alpha_i > 0$ is a constant given in Table 1. z_1, z_2 and z_3 are the estimates of x_1, x_2 and $f(t)$ respectively.

The control scheme is illustrated in the Figure 2 which illustrates that the output of the observer is fed to the sliding surface that can be designed as

$$s = \lambda x_1 + x_2 \approx \lambda x_1 + z_2 \tag{8}$$

where λ is a positive constant and z_2 is the estimate of state x_2 that contribute toward dynamic sliding surface. By taking the derivative of (8), it gives

$$\dot{s} = \lambda x_2 + \dot{x}_2 \tag{9}$$

By inserting the value of $\dot{x}_2$ from (5) in (9), then

$$\dot{s} = \lambda x_2 + f(t) + bu \tag{10}$$

By the virtue of (7), equation (10) can be written as

$$\dot{s} = \lambda z_2 + z_3 + bu \tag{11}$$

By making $\dot{s} \to 0$ the control law can be derived as.

$$u = \frac{1}{b}(-\lambda z_2 - z_3 + u_{sw}) \tag{12}$$

where

$$u_{sw} = -r_1 |s|^{\frac{1}{2}} sign(s) - r_2 \int_0^t sign(s) \tag{13}$$

By inserting the value of u_{sw} the composite control law can be written as

$$u = \frac{1}{b}(-\lambda z_2 - z_3 - r_1 |s|^{\frac{1}{2}} sign(s) - r_2 \int_0^t sign(s)) \tag{14}$$

Traditionally, in order to achieve fast convergence of sliding variable s, the signum functions gains r_1 and r_2 are designed to be proportional to the disturbances in the system. However, these high gains results in long settling time, high overshoot in the sliding variable and chattering in the control input. On the other hand, smaller gain values results in slow convergence. A disturbance estimation and rejection strategy helps in implementing the proposed control law with small

Table 1. Non-linear function parameters.

Parameters	Values
δ	0.9
α_1	0.25
α_2	0.5
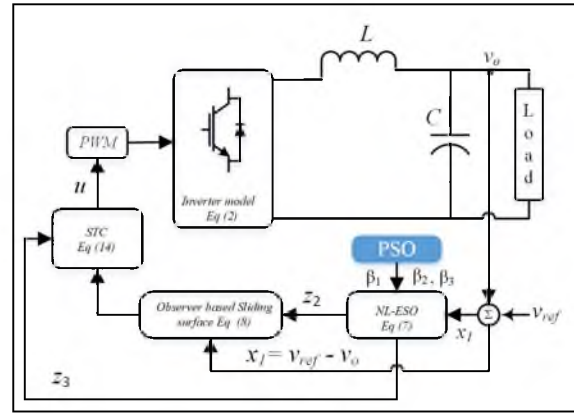
Figure 2. Control strategy.

controller gain without sacrificing the system robustness significantly.

Stability analysis

This section illustrates the stability analysis of the proposed closed-loop system. Firstly, the observer stability is ensured by proving that the error dynamics converge to 0 and then it is proven that the system dynamics and sliding surface converge to 0 in finite time. For that purpose, the observation errors are defined as

$$\left\{ \begin{array}{l} e_1 = z_1 - x_1 \\ e_2 = z_2 - x_2 \\ e_3 = z_3 - f(t) \end{array} \right. \tag{15}$$

As $|f'(t)| = C$ is bounded uncertainty where, C is a constant. By taking the derivative of the estimation error, the observer error dynamics becomes

$$\left\{ \begin{array}{l} \dot{e}_1 = \dot{z}_1 - \dot{x}_1 \\ \dot{e}_2 = \dot{z}_2 - \dot{x}_2 \\ \dot{e}_3 = \dot{z}_3 - \dot{f}(t) \end{array} \right. \tag{16}$$

From (7) and (15), (16) continues to be

$$\left\{ \begin{array}{l} \dot{e}_1 = (z_2 - x_2) - \beta_1 e_1 \\ \dot{e}_2 = (z_3 - f(t)) - \beta_2 e_1 + bu - bu \\ \dot{e}_3 = -\beta_3 fal(e_1, \alpha_2, \delta) + \dot{f}(t) \end{array} \right. \tag{17}$$

Further simplification of (17) results in

$$\begin{cases} \dot{e}_1 = e_2 - \beta_1 e_1 \\ \dot{e}_2 = e_3 - \beta_2 e_1 \\ \dot{e}_3 = -\beta_3 e_1 + \dot{f}(t) \end{cases} \tag{18}$$

By writing in matrix form we get

$$\begin{bmatrix} \dot{e}_1 \\ \dot{e}_2 \\ \dot{e}_3 \end{bmatrix} = \begin{bmatrix} -\beta_1 & 1 & 0 \\ -\beta_2 & 0 & 1 \\ -\beta_3 & 0 & 0 \end{bmatrix} \begin{bmatrix} e_1 \\ e_2 \\ e_3 \end{bmatrix} + \begin{bmatrix} 0 \\ 0 \\ \dot{f}(t) \end{bmatrix} \tag{19}$$

where $|f'(t)| < C$ is bounded and by proper selection of the parameters β_1, β_2 and β_3 the characteristic polynomial for above system $P(s) = |SI - A|$ is made Hurwitz stable which leads the estimation errors e_1, e_2 and e_3 converge to 0 in a finite time.[27] Stability of proposed control law is proven by using Lyapunov stability criteria. Consider a positive definite Lyapunov candidate given by

$$V = \frac{1}{2} s^2 \tag{20}$$

$$\dot{V} = s\dot{s} \tag{21}$$

$$\dot{V} = s(\lambda x_2 + \dot{x}_2) \tag{22}$$

By substituting the value of $\dot{x}_2$ and $u(t)$, then

$$\dot{V} = s(\lambda x_2 + f(t) + bu(t)) \tag{23}$$

$$\dot{V} = s(\lambda x_2 + f(t) + b(-\frac{1}{b}(\lambda z_2 + z_3 - u_{sw})) \tag{24}$$

$$\dot{V} = s(\lambda x_2 + f(t) - \lambda z_2 - z_3 + u_{sw}) \tag{25}$$

$$\dot{V} = s(\lambda(x_2 - z_2) + (f(t) - z_3) + u_{sw}) \tag{26}$$

$$\dot{V} = (\hat{s} + s - \hat{s})(\lambda(x_2 - z_2) + (f(t) - z_3) + u_{sw}) \tag{27}$$

$$\dot{V} \leqslant (|\hat{s}| + |s - \hat{s}|)(\lambda(x_2 - z_2) + (f(t) - z_3) + u_{sw}) \tag{28}$$

$$\dot{V} \leqslant |\hat{s}|(\lambda(x_2 - z_2) + (f(t) - z_3)) + |s - \hat{s}|(\lambda(x_2 - z_2) + (f(t) - z_3)) + |\hat{s}|u_{sw} + |s - \hat{s}|u_{sw} \tag{29}$$

By the virtue of observer convergence, $\dot{V} \leqslant |\hat{s}|(\lambda(x_2 - z_2) + (f(t) - z_3)) + |s - \hat{s}|(\lambda(x_2 - z_2) + (f(t) - (f(t) - z_3)) + |s - \hat{s}|u_{sw}$ is bounded and significantly small which leaves

$$\dot{V} \leqslant |\hat{s}|u_{sw} = |\hat{s}|(-r_1|s|^{0.5}sign(s) - r_2 \int_0^t sign(s)) \tag{30}$$

$$\dot{V} \leqslant |\hat{s}|u_{sw} = -|\hat{s}|\left(r_1|s|^{0.5}sign(s) + r_2 \int_0^t sign(s)\right) \tag{31}$$

$$\dot{V} \leqslant -|\hat{s}|\left(|r_1|s|^{0.5}sign(s)| + |r_2 \int_0^t sign(s)|\right) \tag{32}$$

Equation (32) can be written as

$$\dot{V} < |\hat{s}|u_{sw} = -\eta|\hat{s}| \tag{33}$$

where,

$$\eta = \left(|r_1|s|^{0.5}sign(s)| + |r_2 \int_0^t sign(s)|\right)$$

thus, any positive value for r_1 and r_2 will result in

$$V\dot{V} < 0 \tag{34}$$

This completes the proof.

State convergence

In order to prove the state convergence following Lyapunov candidate function is selected.

$$V = \frac{1}{2}x_1^2 + \frac{1}{2}z_2^2 + \frac{1}{2}z_3^2 \tag{35}$$

Differentiating the above equation gives

$$\dot{V} = x_1\dot{x}_1 + z_2\dot{z}_2 + z_3\dot{z}_3 \tag{36}$$

$$\dot{V} = x_1 x_2 + z_2\dot{z}_2 + z_3\dot{z}_3 \tag{37}$$

$$\dot{V} = x_1(z_2 - e_2) + z_2\dot{z}_2 + z_3\dot{z}_3 \tag{38}$$

$$\dot{V} = x_1 z_2 - x_1 e_2 + z_2\dot{z}_2 + z_3\dot{z}_3 \tag{39}$$

$$\dot{V} = x_1 z_2 - x_1 e_2 + z_2(z_3 + bu - \beta_2 e_1) + z_3\dot{z}_3 \tag{40}$$

By inserting u from (14), then

$$\dot{V} = x_1 z_2 - x_1 e_2 + z_2(z_3 + b$$

$$\left(-\frac{1}{b}(\lambda z_2 + z_3 - r_1|s|^{0.5}sign(s)\right.$$

$$\left.-r_2 \int_0^t sign(s)\right) - \beta_2 e_1) + z_3\dot{z}_3 \tag{41}$$

$$\dot{V} = x_1 z_2 - x_1 e_2 + z_2(z_3 - (\lambda z_2 + z_3 - r_1|s|^{0.5} sign(s)$$
$$- r_2 \int_0^t sign(s)) - \beta_2 e_1) + z_3 \dot{z}_3$$

$$\tag{42}$$

$$\dot{V} = x_1 z_2 - x_1 e_2 - \lambda z_2 z_2 - z_2(-r_1|s|^{0.5} sign(s)$$
$$- r_2 \int_0^t sign(s)) - z_2 \beta_2 e_1 + z_3 \dot{z}_3$$

$$\tag{43}$$

$$\dot{V} \leqslant |x_1 z_2| + |x_1 e_2| + \lambda |z_2 z_2| - \eta |z_2| + \beta_2 |z_2 e_1| + |z_3 \dot{z}_3|$$

$$\tag{44}$$

$$\dot{V} \leqslant \frac{x_1^2}{2} + \frac{z_2^2}{2} + \frac{x_1^2}{2} + \frac{e_2^2}{2} + \lambda z_2^2 + \eta \frac{z_2^2}{2} + \frac{\beta_2 z_2^2}{2}$$
$$+ \frac{\beta_2 e_1^2}{2} + \frac{z_3^2}{2} \beta_3$$

$$\tag{45}$$

By rearranging the terms

$$\dot{V} \leqslant \frac{x_1^2}{2} + \frac{x_1^2}{2} + \frac{z_2^2}{2} + \lambda z_2^2 + \eta \frac{z_2^2}{2} + \frac{\beta_2 z_2^2}{2} + \frac{z_3^2}{2} \beta_3$$
$$+ \frac{e_2^2}{2} + \frac{\beta_2 e_1^2}{2}$$

$$\tag{46}$$

It can be written as

$$\dot{V} \leqslant [2 \quad 1 + 2\lambda + \eta + \beta_2 \quad \beta_3]V + (|e_2| + \beta_2|e_1|)$$

$$\tag{47}$$

this equation can be written in the following form

$$\dot{V} \leqslant KV + L_v$$

$$\tag{48}$$

It is a first order differential equation whose general solution can be written as

$$V(t) = \frac{1}{I(t)} \left[\int I(t) L_v dt + c \right]$$

$$\tag{49}$$

where $I(t)$ is the integral factor given as

$$I(t) = e^{\int -K dt} = e^{-Kt}$$

$$\tag{50}$$

$$V(t) = \frac{1}{e^{-Kt}} \left[\int e^{-Kt} L_v dt + c \right]$$

$$\tag{51}$$

$$V(t) = \frac{1}{e^{-Kt}} \left[\frac{e^{-Kt}}{-K} L_v + c \right]$$

$$\tag{52}$$

For finding the constant c we find the initial conditions

$$V(t) = \frac{e^{-Kt}}{e^{-Kt}} \left[\frac{L_v}{-K} + \frac{c}{e^{-Kt}} \right]$$

$$\tag{53}$$

$$V(t) = ce^{Kt} - \frac{L_v}{K}$$

$$\tag{54}$$

$$V(0) = -\frac{L_v}{K} + c$$

$$\tag{55}$$

$$c = V(0) + \frac{L_v}{K}$$

$$\tag{56}$$

Then (54) can be represented as

$$V(t) = \left[V(0) + \frac{L_v}{K} \right] e^{Kt} - \frac{L_v}{K}$$

$$\tag{57}$$

If K and L_v are bounded, then states will remain bounded in finite time. This completes the proof.

Observer gain tuning

The estimation accuracy of the nonlinear extended state observer is critical to the closed-loop control performance of the system. The greater the convergence rate, the higher the accuracy of the control loop. In this text optimal observer parameters are obtained using particle swarm optimization technique by developing a unique cost function presented in Anjum et al.[28]

The procedure of the PSO is presented in Figure 3(a) where the members of the swarm are represented as particles and each particle provide a potential solution to the estimation error-based objective function. At each iteration, the specified objective function is evaluated for each particle and particles are updated with personal best, *pbest*, and global best, *gbest*, positions which indicate the best solution provided by individual particle and entire swarm, respectively. Before each iteration, particles change their position as follows;

$$\begin{cases} v_i^{k+1} = w v_i^k + c_1.rand_1(..)(pbest_i - x_i^k) \\ \qquad + c_2.rand_2(..)(gbest_i - x_i^k) \\ x_i^{k+1} = x_i^k + v_i^{k+1} \end{cases}$$

$$\tag{58}$$

where v_i^k is the velocity of ith particle at k^{th} iteration, w, c_1 and c_2 are the weighting factors, x_i^k is the current position of the particle i at k^{th} iteration, *pbest* and *gbest* are the optimal solutions given by particle i and entire swarm, respectively, as shown in Figure 3(b). The values of parameters assigned to PSO are listed in Table 2. The primary goal of the proposed control algorithm is to minimize the tracking error x_1 in order to precisely follow the v_{ref} of the VSI. Whereas, the state estimation errors e_1 and e_2 would be small if
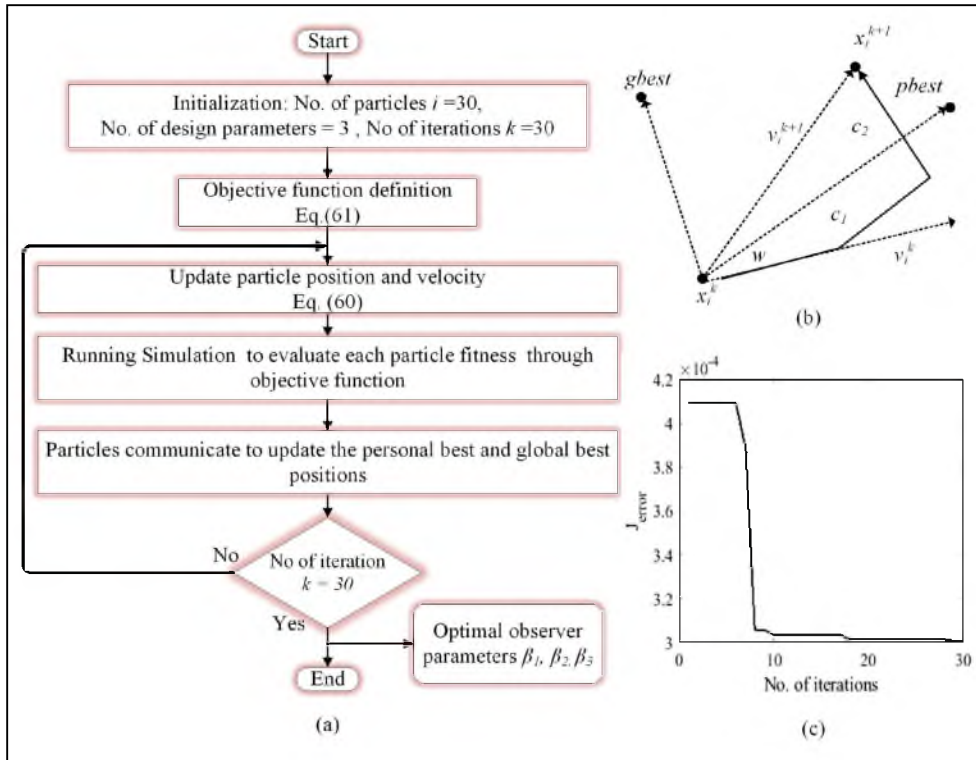
Figure 3. (a) flow chart of PSO algorithm, (b) particles position and velocity update, and (c) PSO convergence.

Table 2. PSO parameters.

Symbol	Description	Values
k	No. of iteration	30
i	No. of particles	30
$\beta_1, \beta_2, \beta_3$	No of designed parameters	3
c_1	Weighting factor	1.42
c_2	Weighting factor	1.42
w	Weighting factor	0.9

the observer gains are optimally designed . For that purpose, the objective function to be evaluated by the swarm particles is specified as

$$J = \int_0^t |e_1| dt + \int_0^t |e_2| dt + \int_0^t |x_1| dt \qquad (59)$$

The PSO will minimize the objective function by selecting the optimal observer parameters β_1, β_2, and β_3 as shown in Figure 3(c), where more accurate estimation of system states are achieved. A comparison of PSO based algorithm and heuristic-based observer gain selection is given in Figures 4 and 5 which clearly depicts that PSO based algorithm exhibits superior performance in terms of both tracking and estimation error minimization. Being the integral part of proposed control law, the precise estimation of system states also
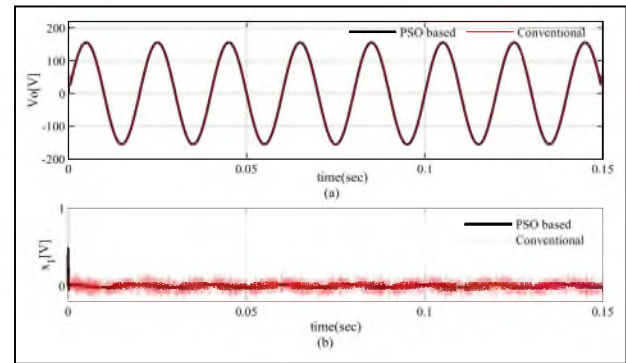

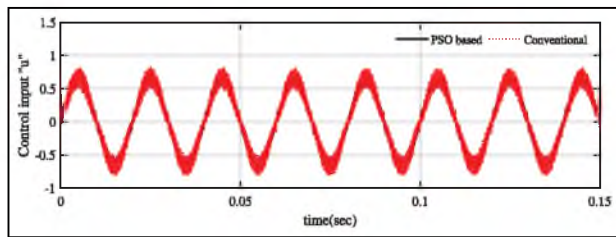**Figure 4.** (a) Output voltage and (b) tracking error.

effectively contributes toward smooth control input as presented in Figure 6.

Simulation results for reference tracking

The effectiveness of the proposed continuous dynamic SMC is validated through MATLAB Simulink. The performance of the proposed controller is compared with the back-stepping controller presented in Diouri et al.[12] The discrete components values used for simulation and designed controllers parameters are presented in Tables 3 and 4, respectively. This study compares the performance of the inverter under three operational
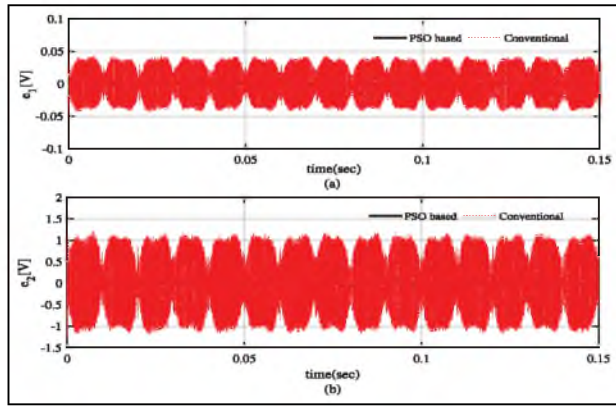
Figure 5. (a) First state estimation error and (b) second state estimation error.

Figure 6. Control input u.

Table 4. Controller parameters.

Symbol	Description	Values
Observer gain	β_1	$1.2e^4$
Observer gain	β_2	$2.917e^7$
Observer gain	β_3	$1.563e^{11}$
Sliding constant	λ	15000
Controller gain	r_1	20
Controller gain	r_1	400
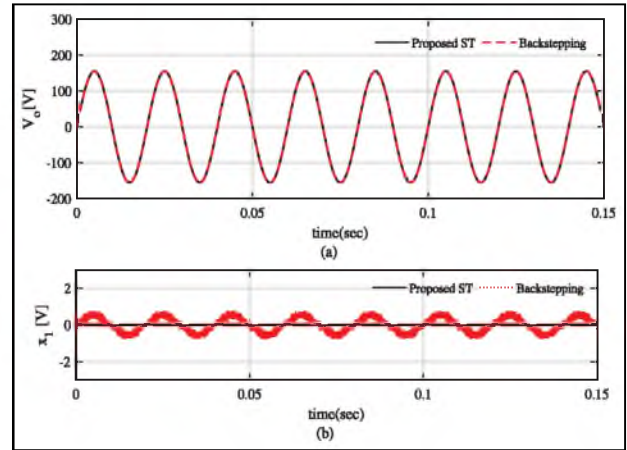
Figure 7. (a) Output voltage and (b) tracking error.

Table 3. Characteristic values used for simulation.

Symbol	Description	Values
Input DC voltage	V_{dc}	$240V$
Reference voltage	v_{ref}	$155\sin(2\pi ft)v$
Inductance	L	$5.4\times10^{-3}H$
Capacitance	C	$20\times10^{-6}F$
PWM switching frequency	f_s	15000
Output frequency	f	50
Sampling time	T_s	$100\mu sec$
Nominal linear load	R	100Ω
Non-linear load	R_s, R_{NL}, C_{NL}	$0.32\Omega, 80\Omega, 3200\mu F$

conditions; at nominal load, sudden linear load variations, and highly non-linear rectifier load.
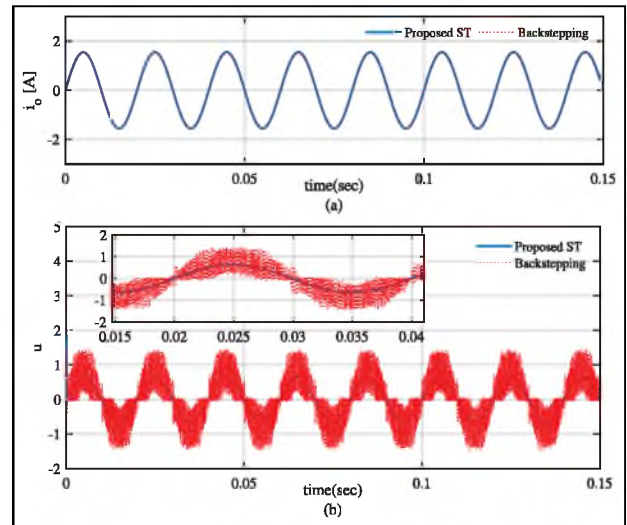
Nominal load

At nominal load, the proposed controller accurately follows the reference voltage and the tracking error immediately converges to 0 as shown in Figure 7(a) and (b), respectively. It is clearly shown in Figure 7(b) that the tracking error for the backstepping controller is $1.4V_{p-p}$ whereas the tracking error for proposed ST-SMC is almost $0V_{p-p}$. The output load current is smooth for both the controllers, as shown in Figure 8(a). Control input is presented in Figure 8(b), which depicts significant oscillations in the backstepping controller while the control input for the proposed

Figure 8. (a) Load current and (b) control input.

controller is relatively smooth and chattering free. The effect of control input is presented in Figure 9 which shows that the smooth inductor current for the proposed ST-SMC, whereas for the backstepping controller, the inductor current is oscillatory.

The state and disturbance estimation errors are presented in described in Figure 10(a) and (b) which shows that the NLESO estimates the system states and disturbance with accuracy. The sliding surface is presented in
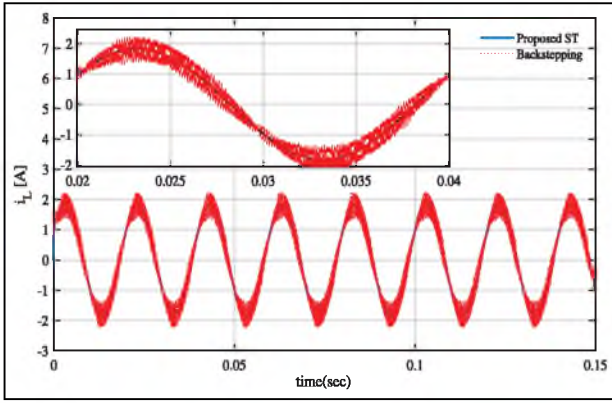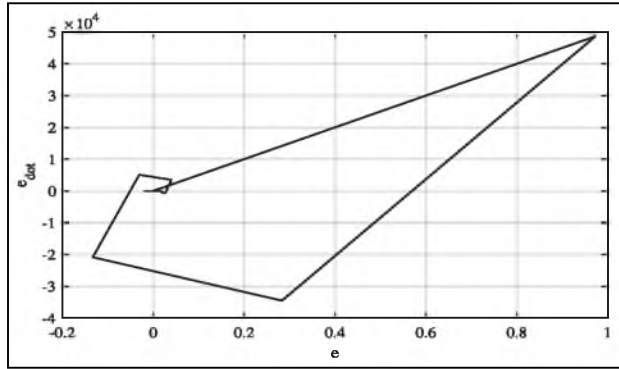
Figure 9. Inductor current.

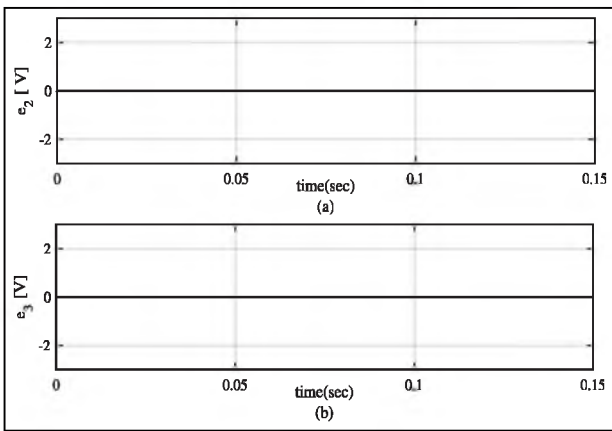**Figure 11.** Sliding surface convergence.

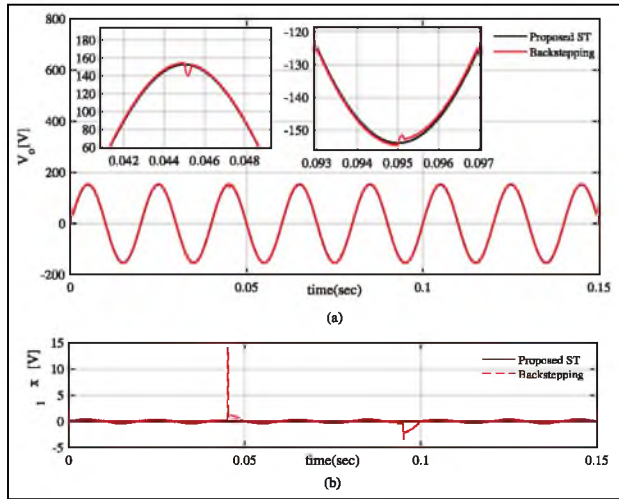**Figure 10.** (a) State estimation error and (b) disturbance estimation error.

Figure 12. (a) Output voltage and (b) tracking error.

Figure 11 which shows that states converge to 0 in a twisting fashion and the steady state error is 0.

Linear load variation

A step variation in the linear load has been made according to (60) where these resistive load variations occur on the system after the system has already reached the steady-state condition. In this case proposed algorithm exhibits excellent tracking performance for output voltage as shown in Figure 12(a) whereas a ripple of $14V_{peak}$ and $4.8V_{peak}$ has been noticed at decreasing and increasing load conditions, respectively for the backstepping controller. The tracking error also converges to 0 in a robust manner for the proposed ST-SMC, while the output ripples are visible for the backstepping controller in Figure 12(b). The sliding surface is presented in Figure 13 which show that the tracking error remains at 0 at nominal load. In contrast, at load variation, a spike of 0.3 V has been observed at both increasing and decreasing loading conditions for the proposed ST-SMC controller. The output load current is presented in Figure 14(a), which shows that the proposed controller shows superior

performance in terms of robustness and settling time is almost 0, whereas the current ripple of $1A$ is visible for the backstepping controller, which also needs some settling time to reach the steady-state. Control input is depicted in Figure 14(b), which is a smooth and continuous for the proposed ST controller, whereas the oscillatory control signal can be observed in the backstepping controller with some abrupt oscillations at the time of load variation.

$$R = \begin{cases} 100\Omega & for \quad t \leqslant 0.045 \\ 50\Omega & for \quad 0.045 \leqslant t < 0.095 \\ 150\Omega & for \quad t \geqslant 0.095 \end{cases} \quad (60)$$

Non-linear load

The inverter's output is connected to a full-wave bridge rectifier, which is common and widely used as a non-linear load for charging batteries as shown in Figure 1. Under this type of load, the proposed ST controller exhibits robust reference tracking capability as shown in Figure 15(a). The rectifier current is smooth, and
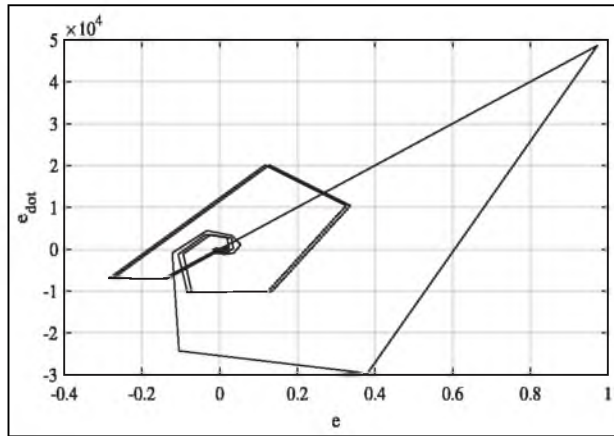
Figure 13. Sliding surface convergence for load variation.
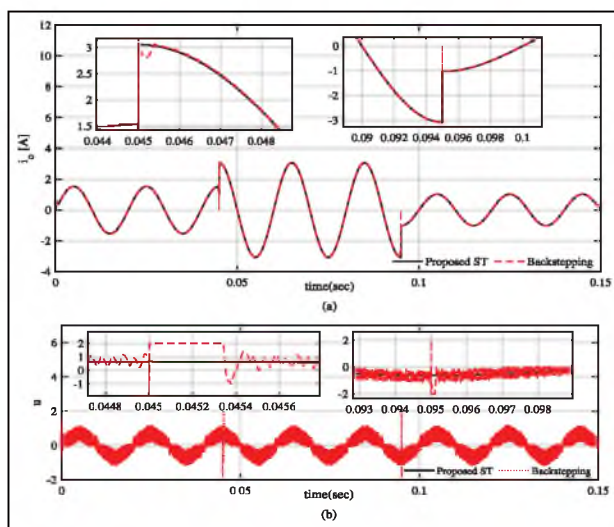

Figure 14. (a) Load current and (b) control input.

tracking error converges to 0 immediately for proposed as presented in Figure 15(b) and (c), respectively. Whereas, for backstepping controller case the tracking error is $1.8V_{p-p}$ and load current settles in $0.02sec$ as presented in Figure 15(b) and (c), respectively.

Total harmonic distortion

The proposed NLESO based STC algorithm exhibit superior performance in terms of harmonic rejection for both linear and non-linear loading conditions. For linear loads, the THD is 0.02% for ST-SMC controller while for the backstepping controller the THD is 0.37% (Figure 16(a) and (b)) and 0.46% for non-linear loads (Figure 16(a) and (b)) respectively. For non-
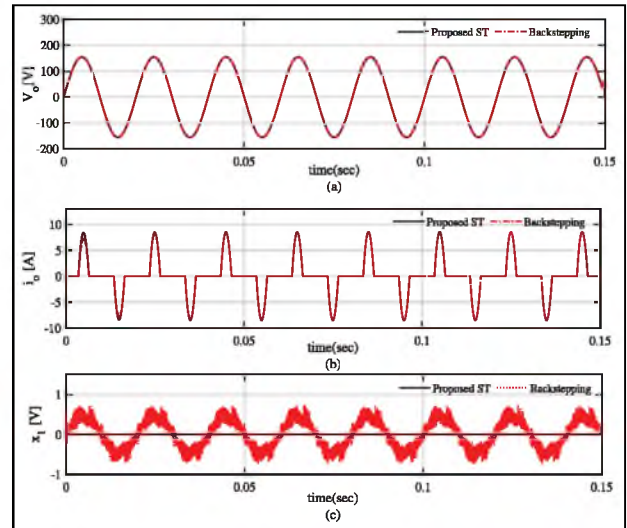

Figure 15. (a) Output voltage, (b) output current, and (c) tracking error.

linear load the THD for proposed ST-SMC controller is 0.08% whereas backstepping controller gives 0.46% as depicted in Figure 16(c) and (d) respectively. Furthermore, a comparison of the proposed algorithm with the previous works is presented in Table 5, reflecting that the proposed controller exhibits superior performance compared to its counterparts.

Conclusion

In this paper, a higher-order SMC of single-phase VSI with non-linear extended state observer has been presented for voltage reference tracking and THD removal against linear and non-linear load disturbances. The proposed observer estimates the lumped parameter disturbances along with system states in the presence of load disturbances. Simultaneously, the complexity of optimal gain design has been removed by using the PSO technique. After the proper estimation of system disturbances, the super twisting controller can be implemented with smaller gain values, reducing the chattering effect and minimizing the THD. The proposed algorithm has been compared with the backstepping controller. The simulation results depict that the designed dynamic ST-SMC controller tracks the reference voltage v_{ref} effectively and the steady-state tracking error remains at $0V$ compared to $1.4V_{peak-peak}$ for the BS control whereas, the THD remains at 0.02% and 0.08% for linear and non-linear loads, respectively, as compared to 0.37% and 0.45% for the BS control algorithm.
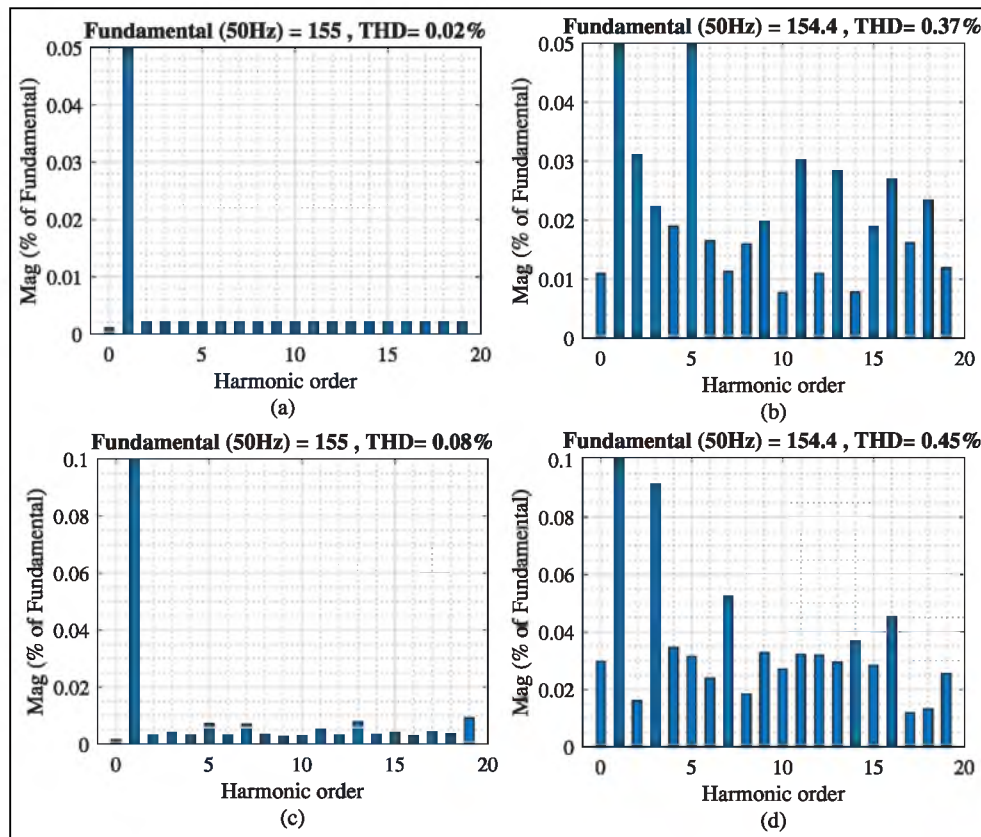
Figure 16. (a) THD at linear load for ST control, (b) THD at linear load for BS control, (c) THD at non-linear load for ST control, and (d) THD at non-linear load for BS control.

Table 5. Proposed SMC and its comparison with other works.

References	Wang et al.[25]	Willmann et al.[29]	Komurcugil et al.[30]	Anjum et al.[28]	Proposed
Controller type	SMC	H_∞	Lyapunov	SMC	ST-SMC
Observer	yes	No	No	yes	Yes
Input *DC* voltage	150	180	400	200	240
Output *AC* voltage (rms)	77.7	110	230	70.7	110
Filter capacitor (μF)	5.25	300	49.404	200	20
Filter inductor (*mH*)	1	1	0.6867	1	5.4
Switching frequency f_{sw}(*kHz*)	15	20	12.5	15	15
Voltage tracking error (*V*)	0.7	1.5	0	0.4	0
THD linear load (%)	0.8	1	0.13	0.20	0.02
THD non-linear load (%)	1.5	12	0.09	1.14	0.08

ORCID iDs

Waqas Anjum https://orcid.org/0000-0003-4284-8141
SM Fasih-ur-Rehman https://orcid.org/0000-0001-7027-7783

References

1. Anjum W, Husain AR, Abdul Aziz J, et al. A robust dynamic control strategy for standalone PV system under variable load and environmental conditions. *Sustainability* 2022; 14(8): 4601.
2. Fei J and Zhu Y. Adaptive fuzzy sliding control of single-phase PV grid-connected inverter. *PLoS One* 2017; 12(8): e0182916.
3. Benhalima S, Miloud R and Chandra A. Real-time implementation of robust control strategies based on sliding mode control for standalone microgrids supplying non-linear loads. *Energies* 2018; 11: 2590.
4. Pichan M and Rastegar H. Sliding-mode control of four-leg inverter with fixed switching frequency for uninterruptible

power supply applications. *IEEE Trans Ind Electron* 2017; 64(8): 6805–6814.

5. Pahlevaninezhad M, Drobnik J, Jain PK, et al. A load adaptive control approach for a zero-voltage-switching DC/DC converter used for electric vehicles. *IEEE Trans Ind Electron* 2012; 59(2): 920–933.

6. Rezkallah M, Sharma SK, Chandra A, et al. Lyapunov function and sliding mode control approach for the solar-PV grid interface system. *IEEE Trans Ind Electron* 2017; 64(1): 785–795.

7. Kumar N, Saha TK and Dey J. Sliding mode control, implementation and performance analysis of standalone PV fed dual inverter. *Sol Energy* 2017; 155: 1178–1187.

8. Benchouia MT, Ghadbane I, Golea A, et al. Design and implementation of sliding mode and PI controllers based control for three phase shunt active power filter. *Energy Proc* 2014; 50: 504–511.

9. Li Z, Zang C, Zeng P, Member S., et al. Control of a grid-forming inverter based on sliding mode and mixed H 2 /H-infinity control. *IEEE Trans Ind Electron* 2017; 64(5): 3862–3872.

10. Yang Y, Lu W and Zhou K. Robust repetitive control scheme for three-phase constant-voltage-constant-frequency pulse-width-modulated inverters. *IET Power Electron* 2012; 5(6): 669–677.

11. Nguyen HT, Kim EK, Kim IP, et al. Model predictive control with modulated optimal vector for a three-phase inverter with an LC filter. *IEEE Trans Power Electron* 2018; 33(3): 2690–2703.

12. Diouri O, Es-Sbai N, Errahimi F, et al. Modeling and design of single-phase PV inverter with MPPT algorithm applied to the boost converter using back-stepping control in standalone mode. *Int J Photoenergy* 2019; 2019: 1–16.

13. Chang EC. Study and application of intelligent sliding mode control for voltage source inverters. *Energies* 2018; 11(10): 2544.

14. Zhu Y and Fei J. Adaptive global fast terminal sliding mode control of grid-connected photovoltaic system using fuzzy neural network approach. *IEEE Access* 2017; 5: 9476–9484.

15. Shtessel Y, Fridman L and Plestan F. Adaptive sliding mode control and observation. *Int J Control* 2016; 89: 1743–1746.

16. Alsmadi YM, Utkin V, Haj-Ahmed M, et al. Sliding-mode control of power converters: AC/DC converters & DC/AC inverters. *Int J Control* 2018; 91: 2573–2587.

17. Kukrer O, Komurcugil H and Doganalp A. A three-level hysteresis function approach to the sliding-mode control of single-phase UPS inverters. *IEEE Trans Ind Electron* 2009; 56(9): 3477–3486.

18. Sabzehgar R, Roshan YM and Fajri P. Modelling and sliding-mode control of a single-phase single-stage converter with application to plug-in electric vehicles. *IET Power Electron* 2019; 12(3): 620–626.

19. Ghanbarian MM, Nayeripour M, Rajaei A, et al. Design and implementation of a new modified sliding mode controller for grid-connected inverter to controlling the voltage and frequency. *ISA Trans* 2016; 61: 179–187.

20. Levant A. Higher-order sliding modes, differentiation and output-feedback control. *Int J Control* 2003; 76: 924–941.

21. Del Pizzo A, Di Noia PL and Meo S. Super twisting sliding mode control of smart inverters grid-connected for PV applications. In: *6th International conference on renewable energy research and applications*, San Diego, CA, USA, 5–8 November 2017, pp.793–796. New York, NY: IEEE.

22. Dai C, Yang J, Wang Z, et al. An enhanced disturbance observer based control for DC-AC inverters using high-order sliding mode. In: *35th Chinese control conference (CCC)*, Chengdu, China, 27–29 July 2016, pp.8601–8606. New York, NY: IEEE.

23. Chang FJ, Chang EC, Liang TJ, et al. Digital-signal-processor-based DC/AC inverter with integral-compensation terminal sliding-mode control. *IET Power Electron* 2011; 4(1): 159–167.

24. Zhu Y, Fei J and Liang X. Sliding mode control of single-phase PV grid-connected inverter. *ICIC Exp Lett* 2017; 5: 1417–1424.

25. Wang Z, Li S, Yang J, et al. Current sensorless sliding mode control for direct current–alternating current inverter with load variations via a USDO approach. *IET Power Electron* 2018; 11(8): 1389–1398.

26. Zhao Z, Yang J, Li S, et al. Continuous output feedback TSM control for uncertain systems with a DC–AC inverter example. *IEEE Trans Circuits Syst II Express Briefs* 2018; 65(1): 71–75.

27. Cao Y, Fu Z, Zhang M, et al. Extended-state-observer-based super twisting control for pneumatic muscle actuators. *Actuators* 2021; 10(2): 35.

28. Anjum W, Husain AR, Abdul Aziz J, et al. Continuous dynamic sliding mode control strategy of PWM based voltage source inverter under load variations. *PLoS One* 2020; 15(2): e0228636.

29. Willmann G, Coutinho DF, Pereira LFA, et al. Multiple-loop H-infinity control design for uninterruptible power supplies. *IEEE Trans Ind Electron* 2007; 54(3): 1591–1602.

30. Komurcugil H, Altin N, Ozdemir S, et al. An extended lyapunov-function-based control strategy for single-phase UPS inverters. *IEEE Trans Power Electron* 2015; 30(7): 3976–3983.